Cytochrome c at Charged Interfaces. 2. Complexes with Negatively Charged Macromolecular Systems Studied by Resonance Raman Spectroscopy†

Peter Hildebrandt*,‡ and Manfred Stockburger

Max-Planck-Institut für Biophysikalische Chemie, Abteilung Spektroskopie, D-3400 Göttingen, FRG

Received December 2, 1988; Revised Manuscript Received April 14, 1989

ABSTRACT: We have analyzed the structure of cytochrome *c* (cyt *c*) bound in a variety of complexes in which negatively charged molecular groups interact with the positively charged binding domain around the heme crevice of cyt *c*. Using resonance Raman spectroscopy, we could demonstrate that these interactions induce the same conformational changes as they were observed in the surface-enhanced resonance Raman experiments of cyt *c* adsorbed on the Ag electrode [Hildebrandt & Stockburger (1989) *Biochemistry* (preceding paper in this issue)]. When cyt *c* is bound to $(As_4W_{40}O_{140})^{27-}$, state II is stabilized, whereas in complexes with phosvitin and cytochrome b_5 state I is formed. The complexes with phospholipid vesicles and inverted micelles reveal a mixture of both states. It is suggested that these systems as well as cyt *c* adsorbed on the Ag electrode may be regarded as model systems for the physiological complexes of cyt *c* with cytochrome oxidase and cytochrome reductase. On the basis of our findings it is proposed that the biological electron-transfer reactions are controlled by electric field induced conformational transitions of cyt *c* upon complex formation with its physiological redox partners.

In this work we continue our studies of cytochrome *c* (cyt *c*)[1] bound to charged interfaces (Hildebrandt & Stockburger, 1989). Our goal is to analyze the effect of electrostatic interactions on the structural and functional properties of cyt by using model systems that may mimic the charged binding domains of its physiological redox partners cytochrome reductase (cyt red) and cytochrome oxidase (cyt ox). In the preceding paper (Hildebrandt & Stockburger, 1989) we used a silver electrode as such a model system. It turned out that cyt *c* adsorbed in the double layer of the electrode can exist in two conformational states. In state I (cyt_I) the native structure of cyt *c* is essentially preserved and the redox potential is the same as for cyt *c* in solution (cyt_N). Compared to the resonance Raman (RR) spectra of cyt_N the SERR spectra of cyt_I reveal only small frequency downshifts by about 1 cm^{-1} for some of the porphyrin modes. These shifts were attributed to an electrochemical Stark effect. In state II (cyt_{II}), however, the heme crevice opens, leading to a thermal- and potential-dependent equilibrium between the six-coordinated low-spin (6cLS) and the five-coordinated high-spin (5cHS) configurations in both oxidation states (Hildebrandt & Stockburger, 1986, 1989). These structural changes give rise to a large negative shift of the redox potential to −0.31 (5cHS) and −0.41 V (6cLS), respectively. Both states, cyt_I and cyt_{II}, can be converted into each other by varying the potential so that the overall redox process of the adsorbed cyt *c* includes three coupled electron-transfer pathways. Evidence was provided that the formation of the different conformers as well as the structure of the individual species is governed by electrostatic interactions with the electrical double layer of the electrode/electrolyte interface and does not result from specific cyt *c*–Ag interactions. Consequently, it was suggested that these conformational states also exist in other systems where cyt *c* is subject to similar electrostatic fields.

In the present work we have tested this conclusion and turned to charged interfaces that are more closely related to biological systems. Using resonance Raman (RR) spectroscopy, we analyzed the structure of cyt *c* bound to heteropolytungstates, inverted micelles, phospholipid vesicles, and anionic proteins. This technique can provide a detailed picture of the structure of the heme group and its interactions with the protein environment (Hildebrandt & Stockburger, 1989). It will be shown that the structural changes of the bound cyt *c* in these systems are in fact similar to those of the adsorbed cyt *c* in the electrode/electrolyte interface, demonstrating that the previous findings have a strong impact on the understanding of the electron-transfer reactions of cyt *c* in general. The biological implications of these results will be discussed.

Materials and Methods

RR spectra were excited with the 413-nm line of a Kr^+ laser (Coherent, 2000 K). The laser power at the sample was 20 mW or less. The spectral slit width was 3.7 cm^{-1} and the calibration accuracy ±0.1 cm^{-1} (Hildebrandt & Stockburger, 1989). For some of the experiments a divided-cell technique was used that is similar to the one described by Rousseau (1981) (Figure 1). This technique permits the quasi-simultaneous measurement of two different samples and thus offers the advantage of being able to detect subtle spectral differences. The samples are deposited in compartments 1 and 2 (0.3-mL volume each) of a divided quartz cell (Hellma) that is rotated through the exciting laser beam. The perpendicu-

† This work was supported in part by the Deutsche Forschungsgemeinschaft.

* To whom correspondence should be addressed.

‡ Present address: Max-Planck-Institut für Strahlenchemie, Stiftstr. 34-36, D-4330 Mülheim, FRG.

[1] Abbreviations: RR, resonance Raman; SERR, surface-enhanced resonance Raman: cyt *c*, cytochrome *c* (the indices I, II, and N denote the conformational states I and II of the adsorbed cyt *c* and the native form of the dissolved cyt *c*); 6cLS, six-coordinated low spin; 5cHS, five-coordinated high spin; 6cHS, six-coordinated high spin; AsT, $(As_4W_{40}O_{140})^{27-}$; AOT, sodium bis(2-ethylhexyl) sulfosuccinate; DOPA, dioleoyl-L-α-phosphatidic acid; PV, phosvitin; cyt b_5, cytochrome b_5; cyt ox, cytochrome oxidase; cyt red, cytochrome reductase; EPR, electron paramagnetic resonance; CD, circular dichroism; MCD, magnetic circular dichroism; NMR, nuclear magnetic resonance.

0006-2960/89/0428-6722$01.50/0

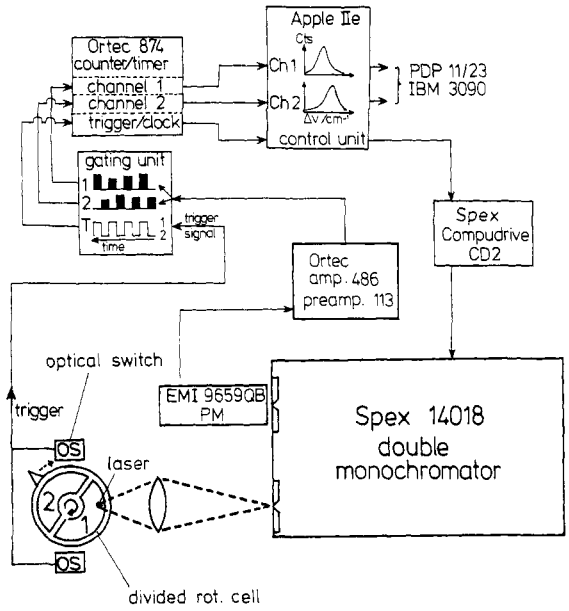

FIGURE 1: Setup of the divided-cell Raman experiments (details are given in the text).

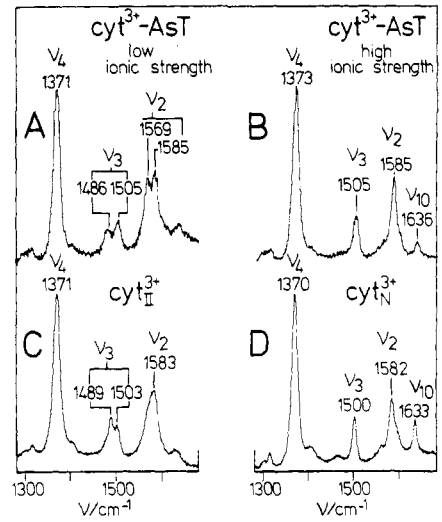

FIGURE 2: RR spectra of cyt^{3+}–AsT at low ionic strength [(A) $I \simeq 10^{-3}$ M] and high ionic strength [(B) $I = 0.03$ M, KCl)] at pH ~6.5 and of cyt_N^{3+} in solution at pH 7.0 (D). (C) shows the SERR spectrum of cyt_{II}^{3+} on the Ag electrode at 0.0 V and pH 7.0 obtained after adsorption at +0.1 V [see Hildebrandt and Stockburger (1989)]. All spectra were excited at 413 nm.

larly scattered light is focused into the entrance slit of the double monochromator, which is equipped with a photomultiplier cooled to −20 °C. The electric signals are normalized and amplified. While the cuvette is rotated, an optical switch (OS; Figure 1) is triggered each time the laser beam passes from one compartment to the other. The trigger signals are used to open and close the gates of channels 1 and 2 of the counter in such a way that they receive only those signals originating from compartments 1 and 2, respectively. When the number of trigger signals, which are accumulated in a third channel of the counter, equals the preset value, the data are transferred to memories 1 and 2 of an Apple IIe computer that serves as storage and controlling unit. Simultaneously, the monochromator is stepped to the next position, and the data acquisition continues. The proper alignment of the optoelectronic device was achieved by a method similar to that of Rousseau (1981).

To obtain a sufficient signal-to-noise ratio, the RR spectra were recorded by repetitive scanning. In general, the total dwell time per monochromator setting was 20–40 s. The so obtained spectra were transferred to a PDP 11/23 for subtraction procedure or to an IBM 3090 for a curve-fitting analysis (Hildebrandt & Stockburger, 1989). Absorption spectra were recorded with a Shimadzu spectrophotometer, Model 240.

K_{27} ($As_4W_{40}O_{140}$) (AsT) was synthesized according to the method of Leyrie and Herve (1978). Inverted micelles of the surfactant sodium bis(2-ethylhexyl) sulfosuccinate (AOT) in octane including cyt *c* were prepared according to the method of Vos et al. (1987). Dioleoyl-L-α-phosphatidic acid (DOPA) was prepared from dioleoyl-L-α-phosphatidylcholine (Sigma). The preparation of the lipid vesicles and the binding of cyt *c* were achieved by a procedure similar to that described by Deveaux et al. (1986). The suspensions, which were buffered to pH 7.0, included a lipid content of about 0.5% and a cyt *c* concentration of 2.5×10^{-5} M so that essentially all the protein molecules were bound.

Cytochrome b_5 (cyt b_5) (detergent free) that was isolated from rabbit liver microsomes was a generous gift of Prof. A. Stier. Phosvitin (PV) was purchased from Sigma and used without further purification. Horse heart cyt *c* (Sigman, type VI) was purified according to the method of Brautigan et al. (1978). All other chemicals were of the highest purity grade available.

Results and Discussion

The common structural property of the model systems studied in this work is a negatively charged surface that is provided by the delocalized charges of the AsT ion, the negatively charged head groups of AOT and phospholipid vesicles, and the anionic amino acid side chains of PV and cyt b_5. These domains strongly interact with the positively charged lysine residues of cyt *c* around the heme crevice to form tight complexes (Chottard et al., 1987; Kimelberg & Lee, 1969; Taborsky, 1970; Salemme, 1976).

Binding of cyt c to Heteropolytungstates. The complexes of cyt *c* with heteropolytungstates have extensively been studied by Chottard et al. (1987) using absorption, CD, and EPR spectroscopies. These authors concluded that the heme iron of the bound cyt *c* can exist in a LS configuration that is different from the dissolved cyt *c* and as well as in a HS configuration. These findings are confirmed by the present RR study. Figure 2 shows the RR spectra in the region of the spin-state marker bands (Hildebrandt & Stockburger, 1989; Parthasarathi et al., 1987). It can be seen that the single bands at 1500 (ν_3) and 1582 cm^{-1} (ν_2) in the RR spectrum of cyt_N^{3+} (Figure 2D), which correspond to the native 6cLS configuration, were replaced by doublets in cyt^{3+}–AsT at low ionic strength (Figure 2A). These doublets obviously represent a mixture of 6cLS and a 5cHS configurations as is concluded from the striking similarities with the SERR spectrum of cyt_{II}^{3+} (Figure 2C) (Hildebrandt & Stockburger, 1989). In state II a thermal equilibrium is established between the 6cLS and the 5cHS configurations. This is reflected, for example, by the doublets of ν_3 with peaks at 1489 and 1503 cm^{-1}. At high ionic strength (Figure 2B) the heme group is nearly completely in the 6cLS configuration as is reflected, for example, by the predominance of the pertinent peaks of ν_3 and ν_2 at 1505 and 1585 cm^{-1}. The frequency shifts of 5 and 3 cm^{-1} of these bands with respect to the related peaks in dissolved cyt_N^{3+} (Figure 2B,D) unambiguously demonstrate that cyt^{3+}–AsT at high ionic strength is different in structure from the dissolved species. Whereas the pure spectrum of the 6cLS configuration in cyt^{3+}–AsT is obtained at high ionic strength (Figure 2B),

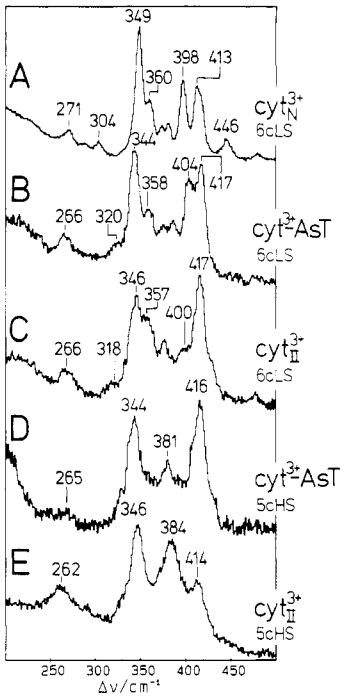

FIGURE 3: RR spectra of cyt^{3+}_N in aqueous solution (A) and of the 6cLS and 5cHS forms of cyt^{3+}–AsT (B, D) compared with the SERR spectra of the 6cLS and 5cHS forms of cyt^{3+}_{II} adsorbed on the Ag electrode. (B), (C), and (D) are difference spectra that were obtained from RR (SERR) spectra measured at different ionic strengths by a subtraction procedure (see text). All spectra were excited at 413 nm.

a spectrum of the 5cHS component can be only obtained by subtracting an appropriate fraction of spectrum 2B from spectrum 2A. Spectra deduced in this way for the fingerprint region are displayed in Figure 3B,D and compared with the related SERR spectra of cyt^{3+}_{II} 6cLS and cyt^{3+}_{II} 5cHS (Figure 3C,E) from the previous study (Hildebrandt & Stockburger, 1989).

The spectra in the frequency range of Figure 3 can be regarded as a fingerprint for the specific heme–protein interactions in cyt *c* (Hildebrandt & Stockburger, 1989). In particular, the bands at 304 and 446 cm^{-1} of cyt^{3+}_N in aqueous solution (Figure 3A) appear to be sensitive indicators for the (native) closed heme crevice. In cyt^{3+}_{II}, however, the protein structure around the heme opening is more loose, which is associated with the weakening and the partial disrupture of the iron–methionine bond. This is reflected by the disappearance of both bands while instead in the 6cLS configuration a new band at 318 cm^{-1} emerges (Figure 3C). The same observations are made in the RR spectrum of the 6cLS form of cyt^{3+}–AsT (Figure 3B). The strong similarities between cyt *c* adsorbed on the Ag electrode and bound to AsT are also seen in the HS forms, whose low-frequency spectra are dominated by three bands around 345, 383, and 415 cm^{-1} (Figure 3D,E). Evidently, the spectra of the adsorbed species are closely related in the 6cLS or in the 5cHS configuration.

Binding of cyt c to Phospholipid Vesicles and Inverted Micelles. The RR spectrum of cyt^{2+} bound to DOPA vesicles (cyt^{2+}–DOPA) is shown in Figure 4B. The complex was prepared by titrating the deaerated cyt^{3+}–DOPA suspension with a concentrated dithionite solution and monitoring the RR band ν_4 for the oxidized (~1370 cm^{-1}) and reduced (~1360 cm^{-1}) forms, respectively. Compared with cyt^{2+}_N (Figure 4A), new features emerged in the ν_3 region constituting a doublet at 1467 and 1491 cm^{-1}. This is characteristic of a mixture of 5cHS and 6cLS configurations (Hildebrandt & Stockburger, 1989), indicating that after binding to DOPA, cyt^{2+} *c* goes from a pure 6cLS form to a mixed-spin configuration. The RR spectrum of cyt^{2+}–DOPA is in good agreement with the SERR spectrum of a 1:1 mixture of cyt^{2+}_{II} and cyt^{2+}_I (Figure 4C).

The RR spectrum of cyt^{3+}–DOPA offers a similar picture as seen in Figure 5. The ν_3 band at 1500 cm^{-1} of cyt^{3+}_N is now replaced by two peaks at 1489 (5cHS) and 1501 cm^{-1} (6cLS)

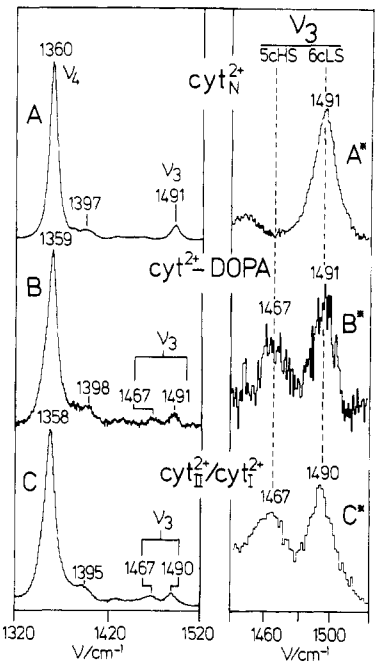

FIGURE 4: RR spectra of cyt^{2+}_N in solution (A) and cyt^{2+} *c* bound to DOPA vesicles (B). (C) is the 1:1 mixture of the SERR spectra of cyt^{2+}_{II} and cyt^{2+}_I adsorbed on the Ag electrode [see Hildebrandt and Stockburger (1989)]. All spectra were measured at pH 7.0. The spectra A*, B*, and C* display an extended view of the ν_3 band region. All spectra were excited at 413 nm.

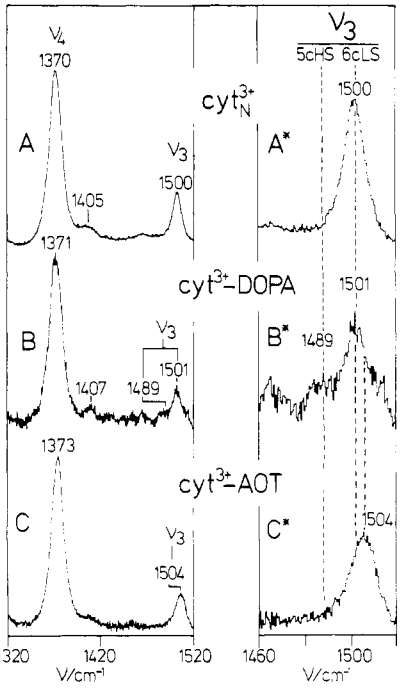

FIGURE 5: RR spectra of cyt^{3+}_N in solution (A), of cyt^{3+} *c* bound to DOPA vesicles (B), and of cyt^{3+} incorporated in AOT micelles in octane at a water/surfactant ratio of 25 (C). All spectra were measured at pH 7.0 and excited at 413 nm. The spectra A*, B*, and C* display an extended view of the ν_3 band region. The Raman bands of octane in (C) [(C*)] were subtracted.

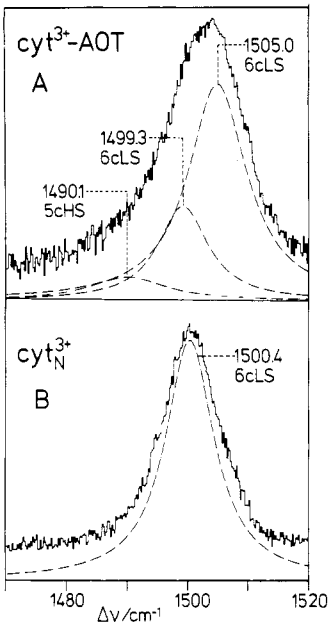

FIGURE 6: RR spectra of cyt^{3+} *c* incorporated into AOT micelles in octane (A) and of cyt_N^{3+} in solution (B) at pH 7.0. The Raman bands of octane were subtracted from spectrum A. The dotted lines are the calculated Lorentz profiles. The spectra were excited at 413 nm.

as was observed for cyt_{II}^{3+} adsorbed on the Ag electrode (Figure 2C). Thus, we can conclude that after binding to phospholipid vesicles, cyt^{3+} and cyt^{2+} are converted to a considerable degree to the conformational state II.[2,3]

The RR spectrum of cyt^{3+} *c* incorporated into inverted micelles of AOT at a H_2O/surfactant ratio of 25 is shown in Figure 5C. The most pronounced spectral difference compared to cyt_N^{3+} (Figure 5A) is the frequency upshift of the peak at 1500 to 1504 cm^{-1}, which is accompanied by a broadening and a decrease of the peak height relative to the 1370-cm^{-1} band. A more careful inspection of this band using a step width of 0.2 cm^{-1} and an improved signal-to-noise ratio revealed the results presented in Figure 6A. While the ν_3 band of cyt_N^{3+} could be well fitted by a single Lorentzian curve (Figure 6B), the asymmetric profile in the RR spectrum of cyt^{3+}–AOT points to more than one component. The curve-fitting analysis revealed three bands at 1505.0, 1499.3, and 1490.1 cm^{-1}. The bands at 1505.0 and 1490.1 cm^{-1} in the RR spectrum of cyt^{3+}–AOT can readily be assigned to the 6cLS and 5cHS forms of cyt_{II}^{3+}. On the other hand, the additional band at 1499.3 cm^{-1} is in excellent agreement with ν_3 of cyt_I^{3+} (1499.5 cm^{-1}). These findings indicate that also cyt^{3+}–AOT exhibits a mixture of the conformational states I and II. Thus, the present study also provides the key for the understanding of the drastic changes in the CD and absorption spectra of cyt^{3+} *c* in AOT micelles [see, for example, Douzou et al. (1979), Pileni (1981), Lysko et al. (1986), Vos et al. (1987), and Brochette et al. (1988)].

Binding of cyt to Phosvitin and Cytochrome b_5. The complex of cyt^{3+} *c* with phosvitin (PV) is formed by mixing cyt^{3+} *c* and PV at a molar ratio of 1:3 in neutral aqueous solution at low ionic strength (I = 0.001 M). The RR spectra of cyt_N^{3+} and the bound cyt^{3+}–PV are very similar (spectra not shown). A band-fitting analysis with Lorentzian line shapes yields values of 1499.8 and 1500.4 cm^{-1} for the ν_3 band of cyt^{3+}–PV and cyt_N^{3+}, respectively, giving a difference of 0.6 cm^{-1}. We also applied the analysis procedure suggested by Rousseau (1981). For the frequency difference of $\Delta\nu$ of two Lorentzian bands of equal intensity I_0 and half-width (Γ) he obtains

$$\Delta\nu = 0.38\left(\frac{I_D}{I_0}\right)\Gamma \qquad (1)$$

where I_0 is the intensity difference between the positive and negative peaks as given in Figure 7. One obtains a value of 0.63 cm^{-1}, in excellent agreement with the band-fitting analysis. Small frequency downshifts are also observed for

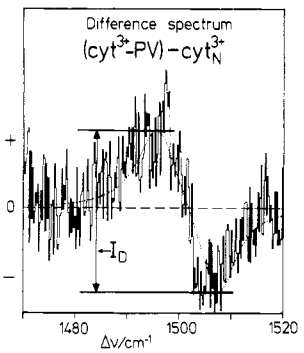

FIGURE 7: Difference spectrum of the RR spectra of cyt^{3+}–PV complex and the dissolved cyt_N^{3+} (413-nm excitation). The dotted line is the calculated profile, and I_D denotes the difference between the positive and the negative peak in this profile.

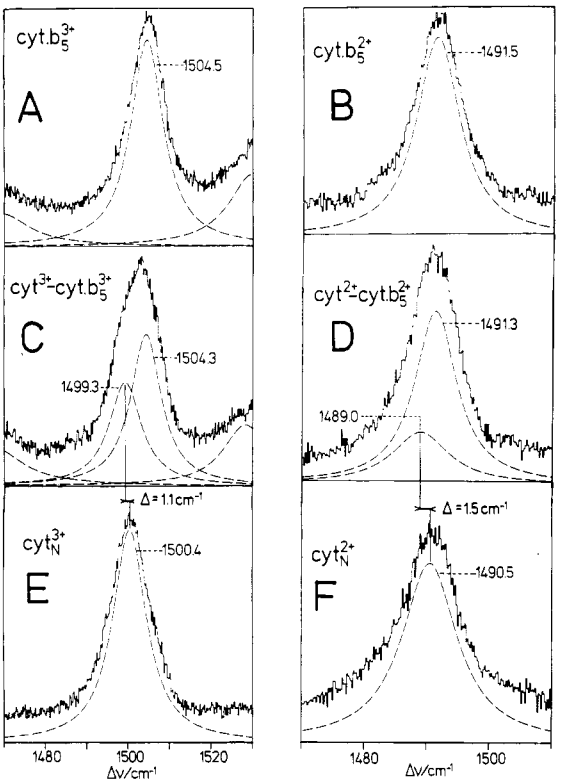

FIGURE 8: RR spectra of cyt b_5^{3+} (A), cyt b_5^{2+} (B), cyt_N^{3+} (E), and cyt_N^{2+} (F) in solution at low ionic strength (I = 0.001 M) at pH 7.0. (C) and (D) display the RR spectra of the 1:1 complexes cyt^{3+}–cyt b_5^{3+} and cyt^{2+}–cyt b_5^{2+}, respectively. The spectra are normalized to equal peak heights. The measured RR intensities of the ν_3 bands of the pure cyt_N^{3+} (E) and cyt_N^{2+} (F) are by a factor of 1.5 and 2.5 lower compared to the ν_3 bands of the pure cyt b_5^{3+} (A) and cyt b_5^{2+} (B), respectively. The dotted lines are the calculated Lorentz profiles. All spectra were excited at 413 nm.

[2] A more detailed RR study reveals that cyt *c* bound to phospholipid vesicles exists in an equilibrium between the conformational states I and II that depends, for example, on the ratio of charged to uncharged head groups (P. Hildebrandt, T. Heimburg, and D. Marsh, unpublished results).

[3] In this context it is interesting to refer to a recent EPR study on the cyt^{3+}–cardiolipin complex by Vincent et al. (1987), who concluded that the structure of the 6cLS form of the bound cyt^{3+} *c* is modified and in addition a weak contribution of HS signals (15%) was detected.

other porphyrin modes (ν_4, ν_{10}) of cyt^{3+}–PV.

The divided-cell technique was also employed to study 1:1 complexes of cyt *c* and cyt b_5 that were prepared according to the method of Mauk et al. (1982). However, the analysis of the spectra was more complicated since in contrast to cyt^{3+}–PV both complex components give rise to RR bands. Figure 8C,D shows the RR spectra in the ν_3 band region of these complexes in the fully oxidized (cyt^{3+}–cyt b_5^{3+}) and fully reduced (cyt^{2+}–cyt b_5^{2+}) forms. They are not identical with the sum of the RR spectra of the individual components (Figure 8A,B,E,F), and the difference spectra (not shown) reveal a similar picture as in the case of cyt^{3+}–PV. This points to small frequency shifts of the ν_3 bands in these complexes. However, the Raman difference technique cannot unambiguously decide which of the ν_3 bands (cyt *c* or cyt b_5) is involved. On the other hand, the band-fitting analysis demonstrates that they are the ν_3 bands of cyt^{3+} and cyt^{2+}, which shift down by 1.1 and 1.5 cm^{-1} (±0.2 cm^{-1}) upon complex formation while the frequencies of the ν_3 bands of cyt b_5^{3+} and cyt b_5^{2+} remain essentially constant.[4] The ν_3 frequencies of cyt^{3+} and cyt^{2+} in the complexes formed with PV and cyt b_5 agree very well with those observed for cyt$_I$ adsorbed on the Ag electrode (Hildebrandt & Stockburger, 1989). This implies that binding of cyt *c* to these proteins stabilizes the conformational state I.

Electric Field Induced Structural Changes in cyt c. cyt *c* is converted to the conformational states I and II after binding to heteropolytungstates, phospholipid vesicles, AOT inverted micelles, and anionic proteins. Thus, the situation is very similar to the "complex formation" of cyt *c* with the Ag electrode covered with specifically adsorbed anions. The distribution between these states differs in the various systems since the charge density is different. DOPA vesicles, AOT micelles, and presumably also AsT exhibit a more or less regular array of negative charges that is closely related to the charge distribution on the Ag electrode surface at potentials far above the potentials of zero charge (Hildebrandt & Stockburger, 1989). In these systems state II prevails. Modifying the electrostatic interactions affects the coordination equilibria in state II and the state I/state II equilibria. This has been observed for cyt *c* adsorbed on the Ag electrode (Hildebrandt & Stockburger, 1989) as well as for heteropolytungstates (Hildebrandt, unpublished results) and phospholipid vesicles.[2]

In the complexes formed with cyt b_5 and PV as well as on the Ag electrode at around –0.4 the stable conformer is state I, suggesting that under these conditions the electrostatic interactions are not strong enough to convert the bound cyt *c* into state II.

It should be mentioned that binding of small anions like phosphate is not sufficient to produce any structural changes in cyt *c*. This can be concluded from the identity of the RR spectra of cyt$_N^{3+}$ in the presence of binding and nonbinding anions. This indicates that a particular arrangement of negatively charged groups is required to induce the transition to state I or II in cyt *c* after complex formation.

So far we have emphasized the similarities of the main structural features of cyt bound in the different complexes, i.e., the spin and coordination states. However, the RR (SERR) spectra of the states II and I are not identical in the various systems. For example, ν_3 varies from 1505.0 to 1503.1 cm^{-1} in cyt$_{II}^{3+}$ 6cLS, from 1490.1 to 1486 cm^{-1} in cyt$_{II}^{3+}$ 5cHS, and from 1499.8 to 1499.3 cm^{-1} in cyt$_I^{3+}$ 6cLS. These spectral differences indicate minor structural changes within the conformers I and II; i.e., they may reflect substates of states I and II as they are known for other proteins (Ansari et al., 1987). Their energy levels may be affected differently in the individual complexes so that, depending on the specific electrostatic interactions, particular substates are predominantly populated. Most likely these substates are associated with slightly different redox potentials.

Taking into account these considerations, the reaction scheme of cyt *c* on the Ag electrode we had derived from the SERR experiments (Hildebrandt & Stockburger, 1989) may provide a qualitative picture for the overall redox process of cyt *c* under the action of electrostatic fields in general.

Biological Implications. Our results support the view that electrodes can be appropriate model systems for biomembranes and the electrical double layers of both systems can apparently exert a similar influence on the structural and functional properties of the adsorbed biomolecules (Bowden et al., 1985). Furthermore, it is concluded that electrodes can mimic the binding domain of proteins or enzymes as far as electrostatic interactions are involved. The main difference between electrode and biological membranes or macromolecules may lie in the desorption process. In the case of cyt *c* at the Ag electrode this is extremely slow (~2 h; Hildebrandt & Stockburger, 1989), whereas, for example, the dissociation of the cyt *c*–cyt b_5 complex is approximately by 4 orders of magnitude faster (Mauk et al., 1982).

In vivo cyt *c* transfers electrons between the enzyme complexes cytochrome reductase (cyt red) and cytochrome oxidase (cyt ox), which both are embedded in the mitochondrial membrane (Wikström et al., 1981; Trumpower & Katki, 1979). It is well established that electrostatic interactions play a dominant role in the reaction of cyt *c* with cyt ox and cyt red (Smith et al., 1977; Speck et al., 1979; Koppenol & Margoliash, 1982; Rieder & Bosshard, 1980). The precursor complexes, cyt–cyt red and cyt–cyt ox, are formed via electrostatic interactions of the negatively charged docking sites of cyt ox and cyt red with the lysine-rich region around the heme crevice of cyt *c*. Similarities between the model systems we had studied in our work and the physiological redox partners of cyt *c* are emphasized not only by the same part of the protein surface serving as the binding domain but also by the strengths of the electrostatic fields in the complexes being comparable. This can be inferred from the binding constants which for cyt/cyt ox (~10^7 M/L; Wikström et al., 1981) lies in the range spanned by the cyt *c*/Ag system (10^9 M/L; Hildebrandt & Stockburger, 1986) and cyt *c* bound to various phospholipid vesicles (3×10^5–10^7 M/L; P. Hildebrandt, T. Heimburg, and D. Marsh, unpublished results). Thus, it is not unlikely that the binding to its physiological redox partners leads to similar structural changes (states II and I) as they were observed in the model systems.

Support for this assumption comes from a recent CD and MCD study on the cyt–cyt ox complex by Weber et al. (1987). These authors demonstrated that the sum of the CD (MCD) spectra of the individual components was not identical with the CD (MCD) spectrum of the cyt–cyt ox complex. From the difference spectra it was concluded that the structures of the heme environment of both cyt *c* and heme a of cyt ox is modified in the complex. In particular, the lack of negative ellipticity of the 417-nm band in the calculated CD spectrum of the bound cyt^{3+} *c* was related to the dissociation of the Fe–methionine bond. Most interestingly, similar observations have been made in the CD spectrum of cyt^{3+}–AsT (Chottard

[4] Attempts to fit the measured spectra by setting the spectral parameters of cyt *c* equal to those of cyt$_N$ and varying only those of cyt b_5 gave significantly higher standard deviations.

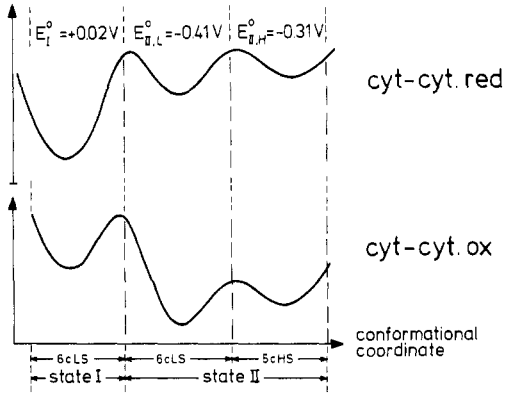

FIGURE 9: Schematic presentation of the potential curves of state I and state II (6cLS and 5cHS) of cyt *c* as postulated for the complexes cyt–cyt red and cyt–cyt ox. E_I^0, $E_{II,L}^0$, and $E_{II,H}^0$ are the redox potentials of cyt_I, cyt_{II} 6cLS, and cyt_{II} 5cHS as determined previously (Hildebrandt & Stockburger, 1989).

et al., 1987), in which cyt^{3+} *c* exists in state II.

Following these considerations we propose a model for the electron transfer reactions of cyt *c* with cyt ox and cyt red that is derived from the analysis of the structural and redox properties of cyt on the Ag electrode and on other model systems. The basic idea of our model is that electrostatic interactions with cyt ox and cyt red induce conformational transitions in cyt *c* that control the physiological electron-transfer processes so that a rapid and unidirectional electron flow is established. We propose that in the complex cyt–cyt ox the conformational state II is stabilized, while in the complex cyt–cyt red state I is thermodynamically favored (Figure 9). This implies that the electron transfer from cyt^{2+} *c* to cyt ox proceeds via state II and is governed by a potential difference of 0.54 V, taking into account the redox potentials of −0.41 V for cyt_{II} 6cLS (Hildebrandt & Stockburger, 1989) and of 0.13 V for heme a, the primary electron acceptor of cyt ox (Wikström et al., 1981). A crude estimation based on classical Marcus theory (Marcus & Sutin, 1985) reveals that this large driving force corresponds to an electron-transfer rate constant for the oxidation of cyt^{2+} *c* that is by 2–3 orders of magnitude larger in state II than in state I (E_0 = +0.02 V).

The situation is different for the reduction of cyt^{3+} *c* by cyt red since the redox potential of heme c_1 (the electron donor of cyt red) is as high as −0.02 V (Trumpower & Katki, 1979). Thus, the largest possible driving force is obtained for the electron-transfer reaction via state I of the bound cyt *c*.

Our model requires that the electrostatic interactions with cyt are different in cyt red and cyt ox and that only in the latter are these strong enough to induce the conversion to cyt_{II}. Under physiological conditions the total electrostatic field results from the charge distribution in the protein/protein interface and from the potential gradient across the mitochondrial membrane. Hence, the proposed different conformational distribution in cyt–cyt red and in cyt–cyt ox implies that the binding sites of these enzymes differ with respect to the arrangement of negatively charged amino acid residues and/or their location in the electrical double layer of the membrane. In this context it is interesting to mention that Koppenol and Margoliash (1982) have estimated that a proper alignment of cyt *c* for the electron-transfer processes requires a significantly lower electric field in cyt–cyt red than in cyt–cyt ox.

The coupling of conformational transitions and electron transfer has recently been stressed by Rush et al. (1988), who investigated the oxidation of cyt^{2+} *c* by tris(1,10-phenanthroline)cobalt(III). These authors provided evidence that the main route of the electron transfer leads via an activated form of cyt^{2+} *c* in which the heme crevice is open. This conformational change was found to depend on the electrostatic potential at the front surface of cyt *c*, and hence it was suggested that this process could be facilitated in physiological redox process. Due to the striking analogies to our experimental findings we ascribe this activated form to state II. Then the increase of the oxidation rate constant in the open form (compared to the closed form) by 4 orders of magnitude (Rush et al., 1988) can qualitatively be understood in terms of the much higher driving force in state II compared to state I.

Our own experimental studies do not provide kinetic data for the conformational transition that could be extended to physiological conditions. Protein dynamics, however, presumably play a crucial role for the electron transfer (Williams, 1988). It may be that rapid conformational changes in the bound cyt *c* control the electron flow. For example, there is strong experimental evidence that the reduction of the Cu_A center in cyt ox leads to a conformational change in cyt ox that can be correlated with a decrease of the electron-transfer rate from cyt^{2+} *c* by several orders of magnitude (Copeland et al., 1987). A possible explanation based on our model is that the structural changes in cyt ox modify the electrostatic interactions with the bound cyt *c*, leading to a population of state I corresponding to a significantly smaller driving force for the electron transfer.

Conclusions

We have demonstrated that the interactions of cyt *c* with large inorganic anions, negatively charged phospholipid vesicles or inverted micelles, and proteins like phosvitin or cytochrome b_5 lead to similar structural changes as for cyt adsorbed on the Ag electrode. This implies that electrodes can be appropriate model systems and SERR spectroscopy a powerful tool to gain more insight into the molecular processes of cyt *c* at charged interfaces in general. On the basis of our findings we have proposed a model for the physiological redox process. This model postulates the coupling of electric field induced conformational changes and electron transfer for the reactions of cyt *c* with cyt red and cyt ox so that a rapid electron flow is facilitated.

Acknowledgments

We thank Prof. A. Weller for encouragement and support. We gratefully acknowledge the purification of cyt by Dr. Sankaram and the preparation of the phospholipid vesicles by T. Heimburg. Cytochrome b_5 was a generous gift of Prof. A. Stier.

References

Ansari, A., Berendzen, J., Braunstein, D., Cowen, B. R., Frauenfelder, H., Hong, M. K., Iben, I. E. T., Johnson, J. B., Ormos, P., Sauke, T. B., Scholl, R., Schulte, A., Steinbach, P. J., Vittitow, J., & Young, R. D. (1987) *Biophys. Chem. 26*, 337.

Bowden, E. F., Hawkridge, F. M., & Blount, H. N. (1985) in *Comprehensive Treatise of Electrochemistry* (Srinivasan, S., Chiznadzhiev, Yu. A., Bockris, J. O. M., Conway, B. E., & Yeager, E., Eds.) Chapter 5, Plenum Press, New York.

Brautigan, D. L., Ferguson-Miller, S., & Margoliash, E. (1978) *Methods Enzymol. 53D*, 131.

Brochette, P., Petit, C., & Pileni, M. P. (1988) *J. Phys. Chem. 92*, 3505.

Chottard, G., Michelon, M., Herve, M., & Herve, G. (1987) *Biochim. Biophys. Acta 916*, 402.

Copeland, R. A., Smith, P. A., & Chan, S. I. (1987) *Biochemistry 26*, 7311.
Devaux, P. F., Hoatson, G. L., Favre, E., Fellmann, P., Farren, B., MacKay, A. L., & Bloom, M. (1986) *Biochemistry 25*, 3804.
Douzou, P., Keh, E., & Balny, C. (1979) *Proc. Natl. Acad. Sci. U.S.A. 76*, 681.
Hildebrandt, P., & Stockburger, M. (1986) *J. Phys. Chem. 90*, 6017.
Hildebrandt, P., & Stockburger, M. (1989) *Biochemistry* (preceding paper in this issue).
Kimelberg, H. K., & Lee, C. P. (1969) *Biochem. Biophys. Res. Commun. 34*, 784.
Koppenol, W. H., & Margoliash, E. (1982) *J. Biol. Chem. 257*, 4426.
Leyrie, M., & Herve, G. (1978) *Nouv. J. Chim. 2*, 233.
Lysko, A. I., Surkov, S. A., Arutyunyan, A. M., Khmel'nitskii, Yu. L., Klyachko, I. L., Levashov, A. V., & Martinek, K. (1986) *Biophysics (Engl. Transl.) 31*, 252.
Marcus, R. A., & Sutin, N. (1985) *Biochim. Biophys. Acta 811*, 265.
Mauk, M. R., Reid, L. S., & Mauk, A. G. (1982) *Biochemistry 21*, 1843.
Parthasarathi, N., Hansen, C., Yamaguchi, S., & Spiro, T. G. (1987) *J. Am. Chem. Soc. 109*, 3865.
Pileni, M. P. (1981) *Chem. Phys. Lett. 81*, 603.
Rieder, R., & Bosshard, H. R. (1980) *J. Biol. Chem. 255*, 4732.
Rousseau, D. L. (1981) *J. Raman Spectrosc. 10*, 94.
Rush, J. D., Koppenol, W. H., Garber, E. A. E., & Margoliash, E. (1988) *J. Biol. Chem. 263*, 7514.
Salemme, F. R. (1976) *J. Mol. Biol. 102*, 563.
Smith, H. T., Staudenmayer, N., & Millet, F. (1977) *Biochemistry 16*, 4971.
Speck, H. S., Ferguson-Miller, S., Osheroff, N., & Margoliash, E. (1979) *Proc. Natl. Acad. Sci. U.S.A. 76*, 155.
Taborsky, G. (1970) *Biochemistry 9*, 3768.
Trumpower, B. L., & Katki, A. G. (1979) in *Membrane Proteins in Energy Transduction* (Capaldi, R. A., Ed.) p 89, Dekker, New York.
Vincent, J. S., Kon, H., & Levin, I. W. (1987) *Biochemistry 26*, 2312.
Vos, K., Laane, C., Weijers, S. R., Van Hoek, A., Veeger, C., & Visser, A. J. W. G. (1987) *Eur. J. Biochem. 169*, 259.
Weber, C., Michel, B., & Bosshard, H. R. (1987) *Proc. Natl. Acad. Sci. U.S.A. 84*, 6687.
Wikström, M., Krab, K., & Saraste, M. (1981) *Cytochrome Oxidase—A Synthesis*, Academic Press, New York.
Williams, R. J. P. (1988) *Z. Phys. Chem. (Leipzig) 269*, 387.

Reversible Independent Unfolding of the Domains of Urokinase Monitored by ^{1}H NMR†

Michael J. Bogusky,‡,§ Christopher M. Dobson,*,‡ and Richard A. G. Smith‖

Inorganic Chemistry Laboratory and the Centre for Molecular Sciences, University of Oxford, South Parks Road, Oxford OX1 3QR, U.K., and Biosciences Research Centre, Beecham Pharmaceuticals, Great Burgh, Yew Tree Bottom Road, Epsom, Surrey KT18 5XQ, U.K.

Received September 27, 1988; Revised Manuscript Received May 1, 1989

ABSTRACT: Human urinary-type plasminogen activator (urokinase) and proteolytic fragments corresponding to the kringle, EGF–kringle, and protease domains have been examined by ^{1}H NMR spectroscopy. The intact protein shows a very well-resolved spectrum for a molecule of this size (MW 54 000), with resonance line widths not greatly increased from those of the isolated domains. On increasing the temperature, the protein at pH values close to 4 was found to undergo two distinct and reversible conformational transitions. These were identified, by comparison with spectra of the proteolytic fragments, as the unfolding of the kringle (and EGF) domains (at ~42 °C) and of a segment of the protease domain (at ~60 °C). The remaining segment of the protease domain showed persistent structure to at least 85 °C at pH 4; only at lower pH values could complete unfolding be achieved. The results indicate that the structures and stabilities of the isolated domains are closely similar to those in the intact protein and suggest that there is a degree of independent motion at least between the kringle and protease domains.

A group of about ten proteins involved in hemostasis and fibrinolysis, including prothrombin, tissue plasminogen activator (t-PA),[1] factor XII, plasminogen, and urokinase (u-PA), have been found to be composed of mosaics of distinct structural domains (Sottrup-Jensen et al., 1978). The latter are classified according to disulfide bridge arrangement and show remarkable homology between the different proteins. They include epidermal growth factor (EGF) like domains, kringle domains, calcium binding domains, and serine protease

† This work was supported in part by the U.K. Science and Engineering Research Council. M.J.B. was supported by a National Science Foundation postdoctoral fellowship (INT-8701333).
‡ University of Oxford.
§ Present address: Merck Sharp and Dohme Research Laboratories, West Point, PA 19486.
‖ Beecham Pharmaceuticals.

[1] Abbreviations: u-PA, urinary-type plasminogen activator; EGF, epidermal growth factor; NMR, nuclear magnetic resonance; t-PA, tissue plasminogen activator; GGACK, L-glutamylglycyl-L-arginine chloromethyl ketone; NpGB, *p*-nitrophenyl *p*-guanidinobenzoate hydrochloride; Tris, 2-amino-2-(hydroxymethyl)-1,3-propanediol.

0006-2960/89/0428-6728$01.50/0